Hindawi Publishing Corporation
International Journal of Photoenergy
Volume 2016, Article ID 5256941, 13 pages
http://dx.doi.org/10.1155/2016/5256941

Research Article

Evaluation of Hydrocalumite-Like Compounds as Catalyst Precursors in the Photodegradation of 2,4-Dichlorophenoxyacetic Acid

Manuel Sánchez-Cantú,[1] Clara Barcelos-Santiago,[1] Claudia M. Gomez,[2] Esthela Ramos-Ramírez,[2] Ma. de Lourdes Ruiz Peralta,[1] Nancy Tepale,[1] Valeria J. González-Coronel,[1] A. Mantilla,[3] and Francisco Tzompantzi[4]

[1]*Facultad de Ingeniería Química, Benemérita Universidad Autónoma de Puebla, Avenida San Claudio y 18 Sur, 72570 Puebla, PUE, Mexico*
[2]*Universidad de Guanajuato, Coonia Noria Alta SIN, 36050 Guanajuato, GTO, Mexico*
[3]*Instituto Politécnico Nacional, CICATA Legaria, Legaria 694, Colonia Irrigación, 11500 Mexico City, Mexico*
[4]*Departamento de Química, UAM Iztapalapa, Avenida San Rafael Atlixco No. 186, 09340 Mexico City, Mexico*

Correspondence should be addressed to Manuel Sánchez-Cantú; manuel.sanchez@correo.buap.mx and Francisco Tzompantzi; fjtz@xanum.uam.mx

Received 10 March 2016; Revised 13 June 2016; Accepted 22 June 2016

Academic Editor: Ying Dai

Three hydrocalumite-like compounds in a Ca/Al ratio of 2 containing nitrate and acetate anions in the interlaminar region were prepared by a simple, economic, and environmentally friendly method. The solids were characterized by X-ray powder diffraction (XRD), thermogravimetric (TG) analysis, nitrogen adsorption-desorption at −196°C, scanning electron microscopy (SEM), infrared spectroscopy (FTIR), and UV-Vis Diffuse Reflectance Spectroscopy (DRS). The catalytic activity of the calcined solids at 700°C was tested in the photodegradation of 2,4-dichlorophenoxyacetic acid (2,4-D) where 57% degradation of 2,4-D (40 ppm) and a mineralization percentage of 60% were accomplished within 150 minutes. The photocatalytic properties were attributed to mayenite hydration, since the oxide ions in the cages are capable of reacting with water to form hydroxide anions capable of breaking down the 2,4-D molecules.

1. Introduction

2,4-Dichlorophenoxyacetic acid (2,4-D) is the most commonly used herbicide in the world and specifically in México [1, 2], where it is used to control wide leaf weeds present in cereal crops although several organizations have recognized it as high toxic pollutant that can induce carcinogen mutations on humans and animals [3, 4]. It belongs to a group of phenolic herbicides that cannot be degraded by conventional methods due to its extremely low biodegradability and it has been detected as a major contaminant in effluents from both subterranean and superficial waters [5, 6]. For these reasons, the scientific community has sought for methods that allow its total degradation.

Nowadays, increased attention has been devoted to the application of photocatalysis as an advanced oxidation process for the elimination of organic pollutants in aqueous wastes using semiconductor materials as photocatalysts. In the scientific literature, TiO_2 has been widely studied among the photocatalytic materials due to its low cost, availability, and its relevant results; however, its low specific surface area and especially the fast recombination of the pair electron hole are constraints that affect its photodegradation activity.

Thus, in recent years other materials such as the layered double hydroxides have attracted considerable attention as a good alternative for the photodegradation of organic compounds.

Layered double hydroxides (LDHs), also known as anionic clays, represent a huge family of materials that exhibit the general formula $[M^{2+}_{(1-x)}M^{3+}_{x}(OH)_2](A^{n-})_{(x/n)}\cdot mH_2O$ where M^{2+} is a divalent cation such as Mg, Cu, and Zn, M^{3+} is a trivalent cation such as Al^{3+} and Fe^{3+}, A^{n-} represents an anion which resides in the interlayer region, and m correspond to the water amount. Their structure resembles that of brucite, where $M^{2+}(OH)_6$ octahedra share edges to build infinite $M(OH)_2$ sheets. Thus, a LDH is created by the partial isomorphic substitution of divalent cations for trivalent ones, in which the layered array is positively charged. This charge is electrically balanced by anionic species located in the interlayer region, along with hydration water molecules.

Currently, LDHs (in particular hydrotalcite and hydrotalcite-like compounds) have been investigated as photocatalyst for the degradation of organic molecules using either UV or visible light radiation. Some examples include the evaluation of binary and ternary compounds such as MgAl [7], ZnAl [8], ZnFe [9], MgFe/TiO_2, [10], ZnCr [11], CuCr [12], MgAlTi [13], ZnAlFe [14], ZnAlLa [15], MgZnAl [16], ZnAlTi [17], and MgZnIn [18].

In this context, the hydrocalumite (HC) and hydrocalumite-like (HCL) compounds belong to a branch of the LDH family which has been scarcely reported in the bibliography in comparison to other LDHs. Their general formula is $[Ca_2M^{3+}(OH)_6](A^{n-})_{(1/n)}\cdot mH_2O$ where M^{3+} is generally an Al^{3+} cation. The layered structure is built by the periodical stacking of positively charged $[(Ca^{2+}, M^{3+})(OH)_6]$ octahedral layers related to brucite and negatively charged interlayers consisting of anions and water molecules. For hydrocalumite, Ca^{2+} and M^{3+}, fixed in a molar ratio of two, are seven- and sixfold coordinated, respectively, being the seventh ligand of the Ca-polyhedron, a water molecule from the interlayer.

In recent times, these compounds have been applied successfully as catalysts precursors in organic reactions such as transesterification [19, 20], aldol condensation [21], cycloaddition [22], isomerization [23], and Meerwein-Ponndorf-Verley [24].

However, although distinct synthesis methods have been proposed in order to prepare HC and HCL compounds [25–29], the coprecipitation method is preferred among the others [19, 22–24, 30–32]. Nevertheless, it should be recognized that this method requires thermal treatments and prolonged aging times to crystallize HC and HCL, together with intensive washing to eliminate undesirable ions. In this sense, all this issues generate environmental, process, and economic drawbacks restricting their large-scale production [33, 34]. An alternative is given by the use of raw materials which do not introduce undesirable anions into the process, adjusting the process variables such as pH, aging temperature, and time. Recently, Valente et al. [33, 34] reported a simple, economic, and environmentally friendly method for hydrotalcite-like compounds' synthesis which can be employed for hydrocalumite's preparation. The advantages of this method include that the final slurry does not require the washing step to eliminate the unreacted ions as is generally performed in the synthesis of these compounds by the coprecipitation method. In addition, the water amount for the preparation of the slurries is reduced to a minimum. Moreover, the use of highly corrosive raw materials and prolonged hydrothermal treatments for crystallization is not required.

It is reported that, upon calcination (higher than 500°C), these materials transform into CaO and mayenite [20]. In this sense, mayenite is considered as an electride (materials that trap electrons at a stoichiometric concentration in the solid state) in which electrons are located in a crystallographic site, not belonging to a particular atom, and behaving like anions and it is considered that such materials could serve as strong reducing agents [35, 36]. In addition, such materials may find application as low-temperature electron emitters. This material is an electrical insulator composed of densely packed, subnanometer-sized cages with positive charge. The unit cell includes two molecules and 12 cages having a free space of 0.4 nm in diameter and can be represented as $[Ca_{24}Al_{28}O_{64}]^{4+} + 2O^{2-}$. The former denotes the lattice framework, and the latter is called "free oxygen ions" that are loosely bound to the cages to compensate the positive charge of the framework [35, 36]. It is well known that during the photocatalytic reactions the negatively charged electrons react with dissolved oxygen to produce hydroxyl radicals which are strong and nonselectively oxidizing agents of organic pollutants. By consequence, mayenite is considered to exhibit potential photocatalytic behavior.

Additionally, it is reported that the pure mayenite phase is obtained at temperatures ~1350°C [37] and although mayenite can be obtained from hydrocalumite-like compounds at temperatures around 500°C it is always accompanied by the CaO phase [20]. In this sense, the incorporation of an organic agent such as the acetate ion could serve as a combustion agent such as the reported combustion method which is based on the principle of explosive decomposition of reagents and fuel mixtures, using the instantaneous heat generated by the chemical reaction between the fuel and metallic precursors to convert the metal ions into the target ceramic material [38, 39].

To our knowledge acetate-containing hydrocalumite-like compounds have been neither synthesized nor employed as catalyst precursors in photocatalysis or even mayenite's viability in this field have been studied. Therefore, in this study three hydrocalumite-like compounds containing nitrate and acetate ions were prepared by a simple, economic, and environmentally friendly method and evaluated as catalysts precursors in the photodegradation of 2,4-dichlorophenoxyacetic acid (2,4-D).

2. Experimental

2.1. Materials' Synthesis. Three hydrocalumite-like compounds containing nitrate (HC-1) or acetate anions (HC-2 and HC-3) in the interlaminar region were synthesized as follows: Technical grade hydrated lime and boehmite were used as calcium and aluminum sources, respectively. The amount of calcium and aluminum sources was fixed in order to achieve a nominal Ca/Al molar ratio of two. 11.85 g of hydrated lime was dispersed at 5000 rpm for 30 min in

250 mL of deionized and decarbonated water (A). Separately, HNO_3 (7.5 mL) or CH_3COOH (4.8 or 9.6 mL) was dissolved in 300 mL of deionized and decarbonated water (HC1, HC2, and HC3, resp.). Then, 5.44 g of boehmite was added to the acid solution and dispersed 5000 rpm for 30 min (B). Thereafter, the product resulting from the addition of (B) to (A) was dispersed at 8000 rpm for 30 min (C). Then, the slurry was aged at 80°C for 3 h with a stirring speed of 300 rpm under a nitrogen atmosphere. After the ageing step the solid was filtered and dried at 60°C overnight. It is important to stress that the samples were not washed at any moment. The acids amounts were established in order to compensate the excess of positive charge caused by aluminum incorporation. In the HC-3 sample the amount of acetic acid was doubled to achieve a 100% acetate anions excess.

2.2. Analytical Methods

2.2.1. X-Ray Powder Diffraction. The X-ray diffraction patterns of the samples were measured in a θ–θ Bruker D-8 Advance diffractometer with CuK_α radiation, a graphite secondary-beam monochromator, and a scintillation detector. Diffraction intensity was measured between 4 and 80°, with a 2θ step of 0.02° and a counting time of 9 s per point.

The identification of the crystalline phases from the XRD patterns was carried out using the JCPDS database and the relative percentages were estimated from the total area under the most intense diffraction peak for each phase identified [40].

Average crystal sizes were calculated by the Scherrer equation $L = K\lambda/(B(\theta)\cos\theta)$ where L is the average crystal size, K is the shape factor (a value of 0.9 was used), λ is the wavelength of Cu Kα radiation, $B(\theta)$ is the Full Width at Half Maximum (FWHM), and θ is the diffraction angle.

Interplanar spacing $d_{(hkl)}$ was calculated from Bragg's law: $n\lambda = 2d_{(hkl)}\sin\theta$, where n is an integer equal to 1, λ is the wavelength of the incident wave, $d_{(hkl)}$ is the spacing between the planes in the atomic lattice, and θ is the diffraction angle.

Since hydrocalumite-like compounds crystallize in a hexagonal lattice cell, the parameter a of the fresh samples was determined from the formula $a = 2d_{(110)}$ using the reflection located at ~31.1. On the other hand, as both CaO and mayenite crystallize in cubic lattices their cell parameter a was calculated from the formulas $a = 2d_{(200)}$ and $a = \sqrt{6}d_{(211)}$, using the reflections found at 37.4 and 18.1 of two theta, respectively.

2.2.2. Fourier Transform Infrared Spectroscopy (FTIR). FTIR spectra were recorded in a PerkinElmer FT1730 spectrophotometer using a nominal resolution of 4 cm^{-1} in order to improve the signal-to-noise ratio.

2.2.3. Thermogravimetric Analysis. Thermogravimetric analyses (TGA) were carried out using a TGAi 1000 series system which was operated under an air flow (20 mL min^{-1}) at a heating rate of 20°C min^{-1} from room temperature to 1000°C. In the determination, ~40 mg of finely powdered dried sample was used.

2.2.4. Scanning Electron Microscopy. Scanning electron microscopy (SEM) analysis was carried out in a JEOL JSM-6610 LV with an acceleration voltage of 20 KeV. Prior to analysis, the sample was covered with gold and mounted over a carbon film. The images were acquired from secondary electron signals.

2.2.5. N_2 Adsorption-Desorption at –196°C. The texture of the calcined samples was analyzed by N_2 adsorption-desorption at –196°C on a Quantachrome Autosorb-3B apparatus. Prior to the analysis, the samples were outgassed in a vacuum (10^{-5} Torr) at 350°C for 12 h. The specific surface areas were calculated by the Brunauer-Emmett-Teller (BET) method, and the pore size distribution and total pore volume were determined by the Barrett-Joyner-Halenda (BJH) method applied to the desorption branch.

2.2.6. UV-Vis Spectroscopy. UV-Vis spectra were acquired using a Cary-100 (Varian) spectrophotometer. The band gap of a material can be estimated from the adsorption edge wavelength of the interband transition. UV-Vis absorption spectra for the different samples were obtained with a Cary-100 Varian spectrophotometer equipped with an integration sphere. The energy band gap (E_g) evaluation for the various samples was calculated from the value obtained by extrapolating the reflectance to the x-axis curve for $y = 0$.

2.3. Photocatalytic Behavior Evaluation. Prior to photocatalytic experiments, an adsorption study of 2,4-D on the annealed solids (700°C) was carried out by mixing the aqueous solution of 2,4-D (40 ppm) with the calcined solids. The extent of equilibrium adsorption was determined from 2,4-D concentration decrease by UV-Vis spectroscopy. Photodegradation of 2,4-D was carried out in a glass batch reactor using 200 mL of a solution containing 40 ppm (1.35 mmol) of 2,4-D g^{-1} catalyst; a protected quartz tube with Pen-Ray power supply (UVP Products) with a typical λ of 254 nm and intensity of 4.4 MWatts cm^{-2} immersed in the solution was used as the source of irradiation. Before irradiation, the solution of 2,4-D and the calcined catalyst were kept for 1 h without irradiation, until the complete adsorption of 2,4-D on the solid and then, the lamp was turned on. The reactor was put simultaneously under irradiation each 30 min for 6 h. After irradiation the solution was filtered and then the solid containing the residual 2,4-D previously adsorbed was analyzed.

The amount of organic carbon present in the solution after reaction was determined with a TOC-V CSH/CSN Shimadzu Analyzer (catalytic oxidation on Pt at 680°C). Calibration runs were performed injecting known amounts of potassium phthalate.

3. Results and Discussion

3.1. X-Ray Powder Diffraction. The X-ray powder patterns of the fresh samples are presented in Figure 1. It was evidenced that all samples exhibited the characteristic reflections of the hydrocalumite-like phase together with calcium carbonate in

Table 1: Cell parameters and average crystal sizes of the fresh samples.

Sample	a, Å	d_1, Å	d_2, Å	d_3, Å	$L_{1(002)}$, nm	$L_{2(002)}$, nm	$L_{3(002)}$, nm	$L_{(110)}$, nm
HC1	5.758	8.896	—	—	41	—	—	55
HC2	5.753	—	8.031	7.551	—	43	40	45
HC3	5.753	—	7.990	7.563	—	39	25	46

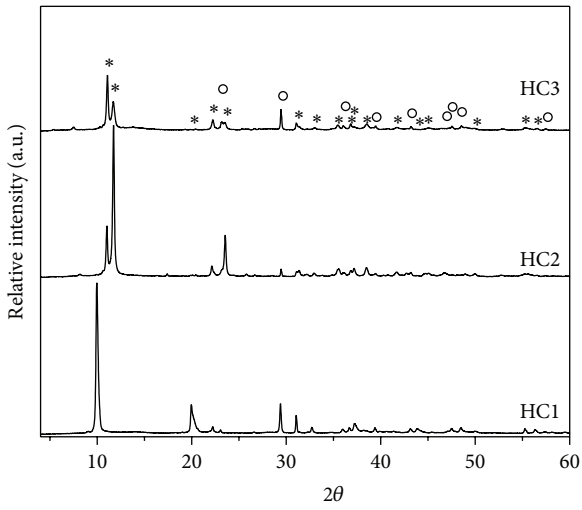

Figure 1: XRD powder patterns of the fresh samples.

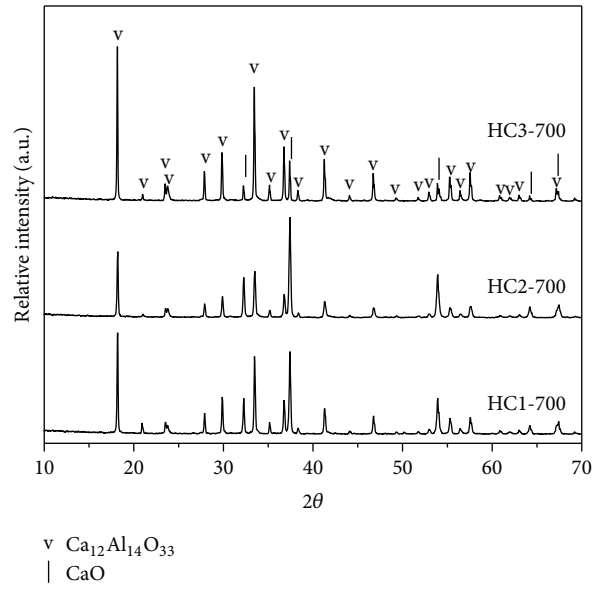

Figure 2: XRD powder patterns of the calcined samples at 700°C.

its calcite form as the main and secondary crystalline phases, respectively. Calcium carbonate presence was attributed to its identification in hydrated lime used as the calcium source. The HC1 sample showed the characteristic reflections of the nitrate-hydrocalumite (JCPDS #89-6723) characterized by a $d_{(002)}$ value of ~8.8 Å (see d_1 at Table 1) [23]. On the other hand, for the HC2 and HC3 samples the ~8.0 Å value (see d_2 at Table 1) was assigned to the flat-lying orientation of the acetate ions [41, 42]. Prevot et al. [41] and Manohara et al. [42] reported a d-spacing within 8.8–8.3 Å for NiAl LDH's which differs about 0.3–0.8 Å with the values obtained in this work. Nevertheless, this difference has been previously observed by Radha et al. [43] and Vieille et al. [44] between hydrotalcite and hydrocalumite-like compounds indicating that the interlayer distance depends not only on the water content, amount, size, orientation, and charge of the anion located between the brucite-like layers [45] but also on the LDH chemical composition.

Similarly, both HC2 and HC3 materials exhibited a $d_{(002)}$ value of ~7.5 Å (see d_3 in Table 1) which according to previous results [25] is assigned to hydrocalumite's carbonate-analogue $[Ca_{0.66}Al_{0.33}(OH)_2](CO_3)_{0.165}{\cdot}mH_2O$. It was evidenced that although special care was taken during materials' synthesis, CO_2 contamination could not be avoided. It is important to stress that the incorporation of acetate ions was favored in the HC3 sample due to the acetic acid excess during the material's synthesis.

On the other hand, the cell parameter a (average cation-cation distance inside the brucite-like layers) of the samples is in good agreement with the reported values of hydrocalumite-like compounds with Ca/Al molar ratio of 2 [46].

Regarding the average crystal sizes (ACS), all samples afforded crystals that grew preferentially in the (110) rather than the (002) planes (see Table 1). Concerning the HC3 sample, it was confirmed that the acetic acid excess caused a hindering effect on the crystallization process since smaller ACS for the (002) crystalline planes were observed.

The X-ray powder patterns of the calcined samples at 700°C are exhibited in Figure 2. Only the characteristic reflections of mayenite (JCPDS #78-0910) and CaO (JCPDS #78-0649) were identified in the calcined samples. Although the same crystalline phases were observed in all samples their relative amounts depended on their chemical compositions. Thus, by means of comparison, the relative crystalline phase content was calculated (see Table 2). The CaO phase was identified as the main crystalline phase in the HC1 and HC2 samples (55 and 67%, resp.) while, on the contrary, the HC3 calcined solid showed only 24%. Even though in the scientific literature CaO obtaining as the main crystalline phase is reported for calcined hydrocalumite-like compounds [19], the high mayenite content disclosed by the calcined HC3 sample was unexpected. In this context, it is reported that pure mayenite is obtained at 1350°C [37] which is, by far, higher than the temperature employed in this work.

Table 2: Cell parameters, average crystal sizes, and relative crystalline phase contents of the calcined samples.

Sample	a, Å^{v}	$L_{(200)}$, nm^{v}	a, Å$^{|}$	$L_{(211)}$, nm$^{|}$	$Ca_{12}Al_{14}O_{33}$%	CaO%
HC1-700	4.805	48	11.946	66	45	55
HC2-700	4.806	42	11.940	54	33	67
HC3-700	4.807	58	11.968	74	76	24

$^{v}Ca_{12}Al_{14}O_{33}$, $^{|}$CaO.

In this sense, this result was attributed to the acetate anions excess which served as a combustion agent such as that reported for the combustion method for ceramic materials' synthesis [38, 39]. For instance, it is reported that during combustion temperatures above 1000°C can be reached for a few seconds [39]. In our case, although combustion was not observed during our solid's annealing, reaction conditions were good enough to achieve mayenite's preferential crystallization. Thus, the higher amount of mayenite found in the HC3 sample compared to the HC2 was attributed to the higher amount of acetate ions introduced in the interlaminar region of the pristine HC3 material.

Cell parameters and average crystal sizes of CaO and mayenite are presented in Table 2. Regarding CaO phase, cell parameter a values (4.805, 4.806, and 4.807 Å for HC1, HC2, and HC3, resp.) were in good agreement with that reported in the JCPDS file (4.805 Å), while the average crystal sizes (ACS), obtained from the (200) reflection, disclosed values of 48, 42, and 58 nm, in that order. The highest ACS given by the calcined HC3 sample was assigned to acetate ions presence which, during annealing, caused a higher crystallization degree compared to the other samples. On the other hand, mayenite's cell parameter a values differed from that reported in the JCPDS file (11.98 Å) which can be attributed to a calcium deficiency generated by CaO formation. By consequence, the calcined HC3 sample, where a lower CaO amount was found, presented a closer value (11.968 Å) than those exhibited by HC1 and HC2.

3.2. Infrared Analysis. Figure 3 shows the mid-infrared spectra of the fresh hydrocalumite-like compounds while Table 3 presents bands' wavenumbers and their assignations. For the nitrate-hydrocalumite (HC1), the absorption bands located in the 3661–3319 cm^{-1} range corresponded to the stretching vibrations of interlayer water and OH groups (see Table 3), respectively [47], while the band observed at 1641 cm^{-1} was assigned to H-O-H bending vibration of the interlayer water molecules, which are strongly hydrogen bonded. Nitrate ions presence in the interlaminar region was corroborated by the band at 1385 cm^{-1} corresponding to the symmetric stretching mode of the nitrate ions [48]. The signals situated at 1460, 1070, and 873 cm^{-1} were attributed to the antisymmetric stretching [49], ν_1 stretching [50], and the bending carbonate vibration, respectively. The presence of these signals was ascribed to the CO_2 captured from air during the HC preparation and calcite identified in the XRD section. Finally, the structural bands at 900–600 cm^{-1} were responsible for the stretching vibrations modes of M-OH, M-O-M, and O-M-O bonds, where M means metal atoms and O indicates oxygen atoms [51].

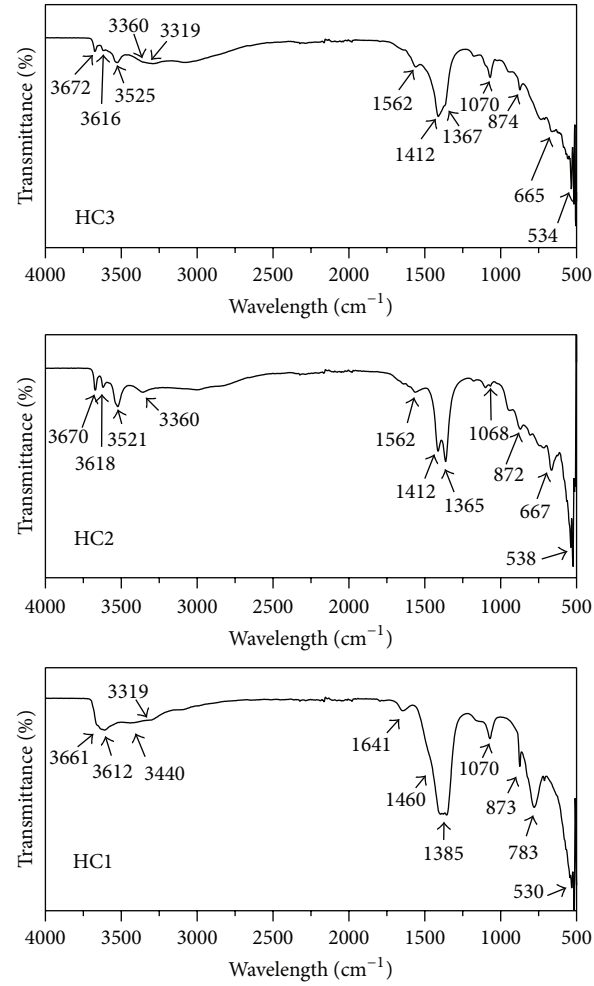

Figure 3: FTIR spectra of the pristine samples.

The analysis of the HC2 and HC3 samples indicated that, besides practically the same infrared bands (except for those at 1641, 1460, 1385, 1070, and 873 cm^{-1}), they exhibited three additional bands observed in the range 1600–1250 cm^{-1}: the first two were located at 1562 and 1412 cm^{-1} which corresponded to COO antisymmetrical and symmetrical stretching vibrations [52] while the third one, around 1365 cm^{-1}, was assigned to carbonate ν_3 stretching mode [50]. It is worthwhile to mention that the identified signals at 1562 and 1412 corroborated the incorporation of the acetate ions

Table 3: Wavenumbers and assignations of the bands of the samples.

HC1	HC2	HC3	Assignation
3661, 3612, 3440, 3319	3670, 3618, 3521, 3360	3672, 3616, 3525, 3319, 3360	Stretching vibration of water and hydroxyl groups
1641	—	—	H-O-H bending vibrations of the interlayer water molecules ($\nu_2 H_2O$)
—	1562, 1412	1562, 1412	COO antisymmetrical and symmetrical stretching vibrations
1460	—	—	Antisymmetric C=O stretching carbonate vibration
1385	—	—	Symmetric stretching mode of the nitrate ions
—	1365	1367	C=O stretching (ν_3)
1070	1068	1070	C=O stretching (ν_1)
873	872	874	Carbonate bending vibration (ν_2)

inside hydrocalumites' structure which is in good agreement with the XRD results (see Figure 1).

3.3. Thermogravimetric Analysis. The TG and the first derivative curves of the fresh samples are shown in Figures 4(a) and 4(b), respectively, while in Table 4 the weight loss percentages and thermal transition intervals are presented. The HC1 exhibited presented a total weight loss of 42.94% and 5 well-defined thermal weight losses, located in the 25–189, 189–375, 375–624, 624–774, and 774–1000°C ranges.

The first weight loss is generally related to the elimination of inter and intraparticle pore water formed by capillary condensation between HCL crystallites and adsorbed surface water bound to gallery and external surfaces [53]. In the next two transitions (189–624°C), the weight loss percentage was assigned to the simultaneous elimination of the calcium-bounded water, dehydroxilation, and denitrification [54]. The last two events were attributed to the total dehydroxylation and anion decomposition.

Similarly to HC1 sample, both HC2 and HC3 materials, where acetate and carbonate ions were identified, presented 5 weight losses (see Table 4). Nevertheless, HC2 and HC3 weight losses were found at distinct intervals and corresponded to different mass elimination. For instance, the first weight loss (attributed to physorbed water elimination) was found in the 25–225°C range with peaks maxima at 188 and 167°C for HC2 and HC3, respectively, indicating a stronger interaction of these compounds with physisorbed water compared with HC1 (112°C). The second and third degradation stages (189–672°C range) are attributed to the interlaminar structure collapse releasing a variety of products where according to Kandare and Hossenlopp [55] they include water, acetic acid, acetone, and carbon dioxide produced from the laminae dehydroxylation and acetate/carbonate ions decomposition. It is worthwhile to mention that the HC2 compound presented higher peaks maximum compared to the HC3 sample which is assigned to the higher acetate anions incorporation in the latter which are less thermally stable compared to the nitrate and carbonate ions. Finally, the last

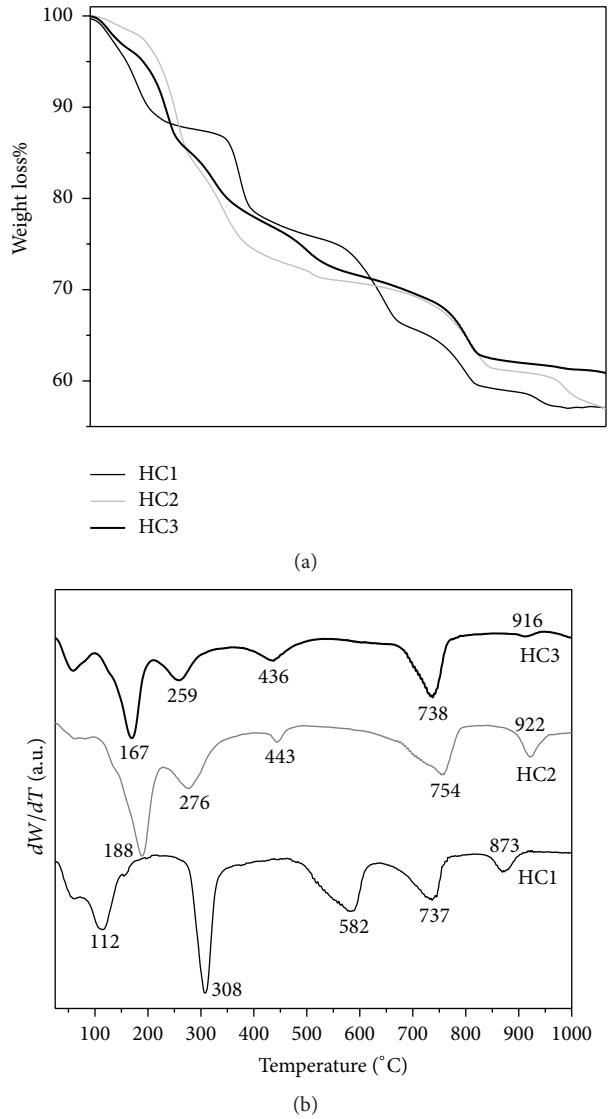

Figure 4: Thermogravimetric analysis results: (a) TG and (b) 1st derivative curves.

Table 4: Thermogravimetric analysis results.

Sample	Thermal transition range (°C)					Total mass loss %
	1st	2nd	3rd	4th	5th	
HC1	25–189 (12.02%)	189–375 (10.71%)	375–624 (11.29%)	624–774 (6.67%)	774–1000 (2.25%)	42.94
HC2	25–225 (16.40%)	225–387 (10.59%)	387–672 (4.68%)	672–793 (7.03%)	793–1000 (4.32%)	40.53
HC3	25–207 (14.58%)	207–376 (8.74%)	376–673 (8.00%)	673–791 (6.30%)	791–1000 (1.52%)	39.32

two observed thermal events identified in the 624–1000°C range were attributed to the total dehydroxylation and anion decomposition. Only one common decomposition peak was identified in all samples (~737–754°C) which was attributed to calcite decomposition [56].

3.4. Scanning Electron Microscopy. Figure 5 presents the SEM images of the fresh (a) and calcined (b) samples. Concerning the fresh samples all of them showed the characteristic plate-like habit of anionic clays. In this sense, only HC1 presented well-defined hexagonal particles while HC2 and HC3 due to their compaction did not present any discernible morphology. On the other hand, upon calcination the original morphology of the fresh samples was completely destroyed giving rise to both plate-like and semispherical particles, the latter being very similar to those reported for CaO [57] and mayenite particles [58]. This result is in good agreement with the XRD results where CaO was observed as the main crystalline phase (HC1 and HC2). It is worth mentioning that the spherical particles were more obvious in the HC1 and HC2 samples. We noticed that sintering was identified in all samples giving rise to an Ostwald ripening effect which involves the growth of larger particles at the expense of smaller ones [56]. However, sintering was more evident in the HC3 sample where the spherical particles were practically absent and larger particles obtaining was noticed. This result matches the highest average crystal sizes disclosed by the calcined HC3 sample compared to HC1 and HC2 (see Table 2). As mentioned in the XRD section, sintering promotion was attributed to acetate groups' combustion during annealing.

3.5. Textural Properties. The nitrogen adsorption-desorption isotherms of the calcined samples are shown in Figure 6 and the corresponding BJH pore size distributions are depicted in the inset. All samples presented type IV isotherms according to IUPAC classification, which is characteristic of mesoporous solids. Conversely, the hysteresis loops corresponded to H3 type which is attributed to plate-like particles aggregates giving rise to the presence of slit-shaped pores of nonuniform size and shape [59]. These results match the SEM analysis where plate-like and semispherical particles were identified. It was observed from the pore size distribution plots (Figure 6 inset) that the samples showed broad bimodal pore size distributions in the micro- and mesopore range, between 1.5 and 7 (HC1 and HC2) and 3 and 20 Å (HC3), and 20 and 200 Å, correspondingly.

Specific surface areas (SSA), pore volumes, and average pore sizes of the annealed samples can be observed in Table 5. The samples exhibited SSA values between 8 and 14 $m^2\,g^{-1}$ which are in good agreement with previously reported results [60] while pore volumes oscillated between 0.041 and 0.068 $cc\,g^{-1}$ for HC2 and HC3, respectively. Regarding the average pore sizes, no significant differences were observed among the samples.

3.6. Band Gap Determination. Band gap energies (E_g) of the calcined materials were determined by UV-Vis diffuse reflectance (Table 5 and Figure 7) using

$$E_g\ (\text{eV}) = 1239\left(\frac{b}{-a}\right), \tag{1}$$

where a and b are coefficients that were linearized in the appropriate region of the spectrum.

E_g values ranged from 3.2 to 3.4 eV which are comparable to those reported for anatase TiO_2 and ZnO (3.0–3.2 and 3.37 eV, resp.) [61–63]. In this sense, it is remarkable that after annealing the calcined solids exhibited similar semiconductive properties although distinct interlaminar ions were introduced in the pristine solids. The semiconductive properties of the LDHs observed after a thermal treatment have been also reported by other authors where they attributed this effect to a solid solution production which creates a new band structure [63]. However, in our case we ascribed materials' semiconductive properties to mayenite's production.

3.7. Photocatalytic Activity. Figure 8 presents the results acquired from the photolysis evaluation (without catalyst) of a 40 ppm 2,4D aqueous solution where it was observed that the 2,4-D molecule was not destroyed even after 120 minutes of UV irradiation. Nevertheless, when photodegradation evaluation was carried out in the presence of the calcined catalysts degradation percentages of 46, 54, and 57% (HC1, HC2, and HC3, resp.) were verified after 150 minutes. These differences can be explained in terms of the band gap energy values differences since, as shown in Table 5, the calcined materials HC2 and HC3 showed comparable energy gap values to that disclosed by titanium dioxide in its anatase phase while calcined HC1 material presented a prohibited energy value of 3.4 eV. In addition, it should be emphasized that the most active material, calcined HC3, was the one with the highest surface area (14 $m^2\,g^{-1}$), providing a larger contact area with the molecule thus favoring the catalytic reaction.

Figure 9 shows the kinetic study of 2,4-D photodegradation with the calcined hydrocalumite-like compounds. As can be seen, the evaluated materials showed an acceptable linearity that was adjusted assuming pseudo-first-order kinetics. The results showed a rate constant maximum for the calcined

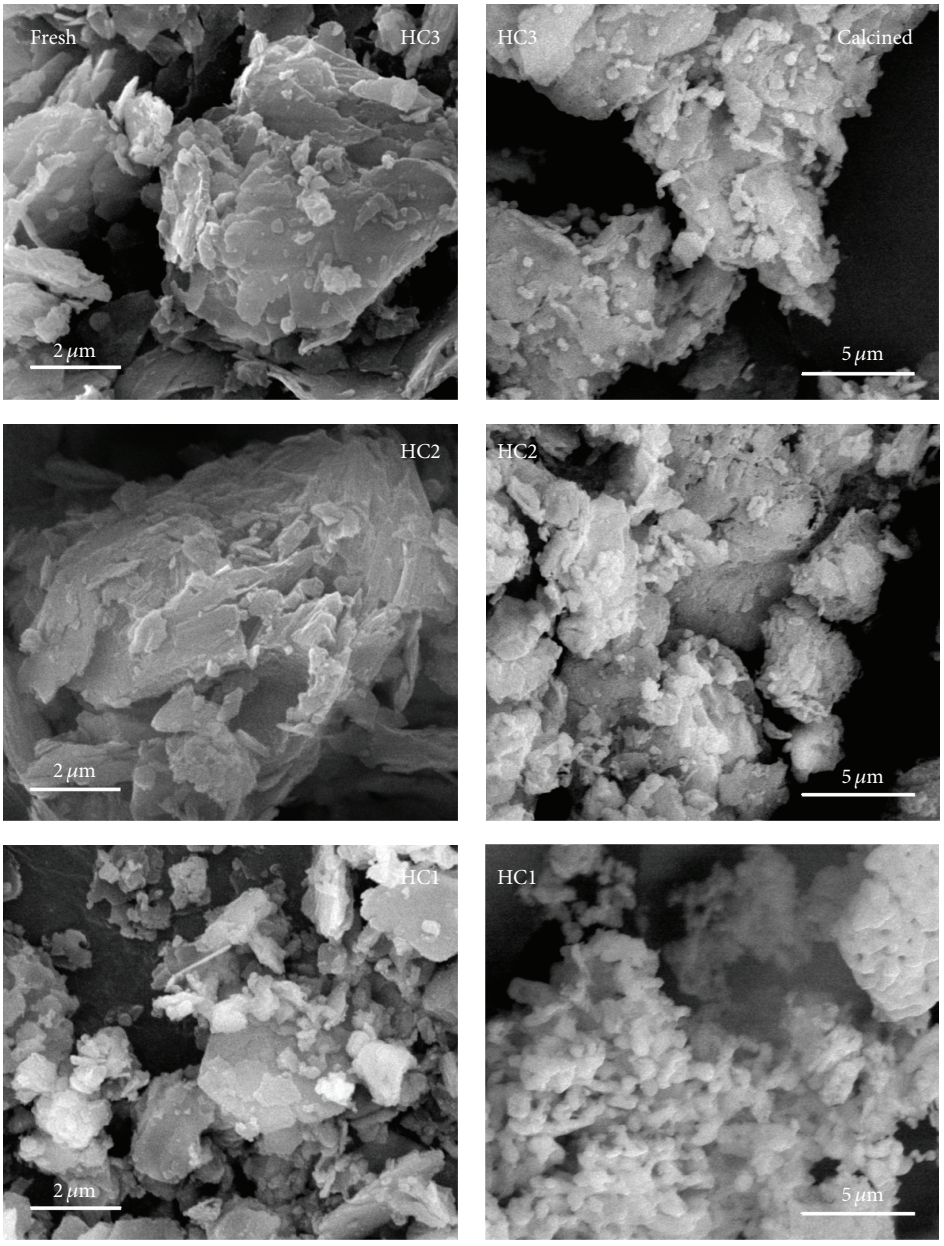

Figure 5: SEM images of the fresh and calcined samples.

HC3 sample ($k_{app} = 57 \times 10^{-3}$ min) and a minimum for the HC1 sample ($k_{app} = 3.2 \times 10^{-3}$ min) which can be explained in the above-discussed terms.

2,4-D mineralization was confirmed by Total Organic Carbon (TOC) analysis (see Figure 10). Figure 9 and Table 5 present the TOC profiles and $t_{1/2}$ obtained after 150 minutes of irradiation, respectively. It was observed that the HC2 and HC3 calcined samples were more active in 2,4-D photodegradation since TOC values were 40 and 60%, in that order. On the other hand, the HC1 calcined sample showed a low mineralization (15%) which was attributed to the physicochemical properties of this material (highest E_g value, low specific surface area, low mayenite content, etc.), which are crucial in the formation of hydroxyl radicals. Moreover, it could be assumed that its crystallographic characteristics prevent adequate separation of charges encouraging recombination of the electron and hole pairs compared to HC2 and HC3 calcined samples diminishing photodegradation effectiveness since recombination prevents the formation of superoxide radical (O_2^-) and hydroxyl radicals (OH^-) which are the initiators of advanced oxidation processes.

On the other hand, it was interesting to notice that although the HC2 calcined sample presented the lowest mayenite amount it exhibited the smallest mayenite average

Table 5: Textural properties, band gap energies, and photocatalytic behavior of the calcined materials.

Sample	BET, $m^2\ g^{-1}$	Pore volume, $cc\ g^{-1}$	Average pore diameter, nm	Band gap energy (eV)	$k_{app} \times 10^{-3}$	$t_{1/2}$ min	TOC%
HC1	10	0.049	19	3.4	3.2	216	15
HC2	8	0.041	21	3.3	46	150	40
HC3	14	0.068	19	3.2	57	121	60

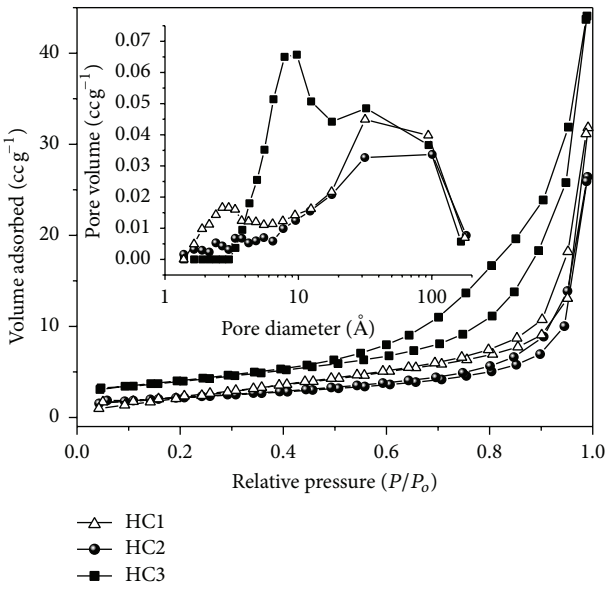

Figure 6: N_2 adsorption-desorption isotherms of calcined solids. Pore size distributions are shown in the insert.

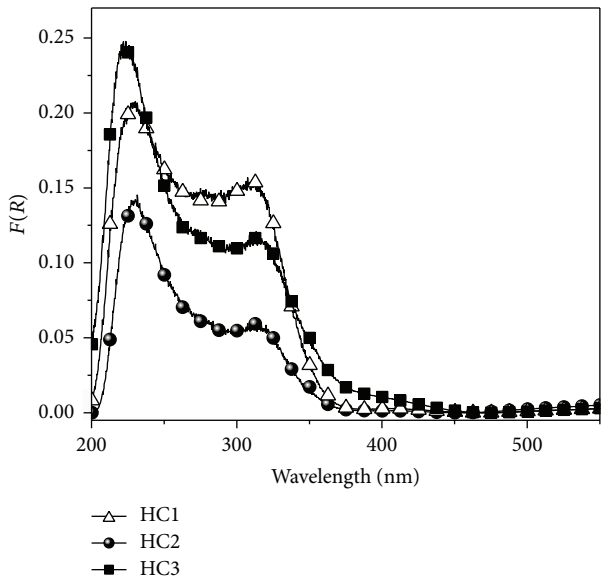

Figure 7: UV-Vis spectra of the calcined samples at 700°C.

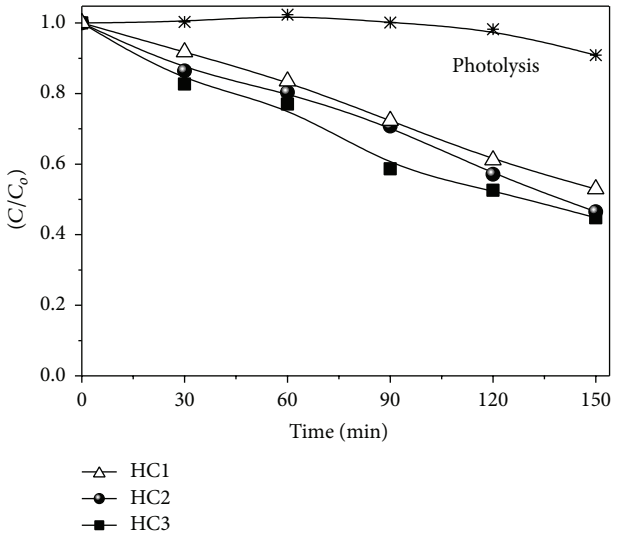

Figure 8: Relative concentrations (C/C_o) versus irradiation time (t) of 2,4-D photodegradation.

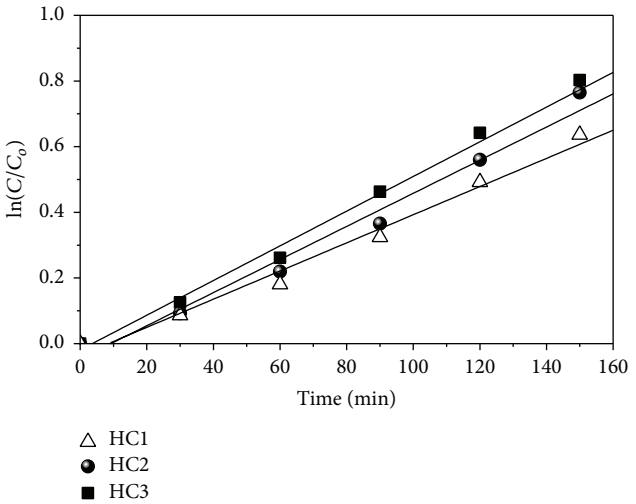

Figure 9: Reaction kinetics of 2, 4-D photodegradation.

crystal size, the highest average pore diameter, and a similar E_g value compared to the HC3 calcined material. These results indicate that a relationship between the chemical composition, crystallographic characteristics, and textural and optical properties is of paramount importance for producing an active material.

As mentioned earlier, these materials have not been previously used as photocatalysts. However, it has been demonstrated by the UV-Vis characterization that the calcined hydrocalumite-like compounds presented similar band gap values compared to those disclosed by anatase and ZnO and are also capable of degrading organic molecules;

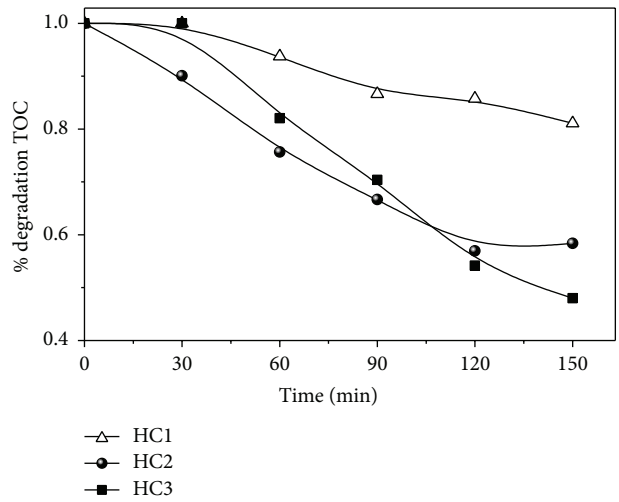

Figure 10: Determination of the Total Organic Carbon (TOC) of the 2,4-D photodegradation.

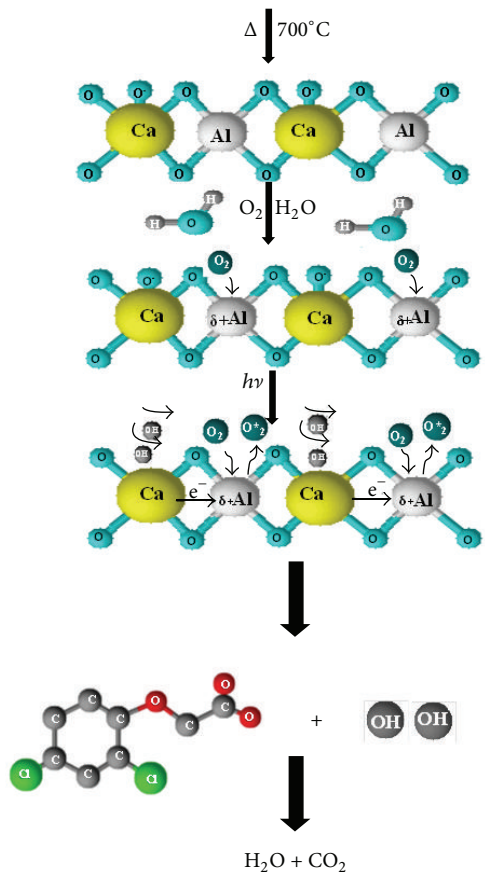

Figure 11: Proposed reaction mechanism.

therefore, a reaction mechanism is proposed (see Figure 11 and (2)–(8)).

As evidenced by the XRD analysis of the calcined samples when a hydrocalumite-like compound is subjected to a thermal treatment under oxidative conditions the structure of the mayenite is obtained (see (2)) favoring the arrangement of surface charges and the mobility of the adsorbed species (see (3)) through the catalyst surface so the exchange of electrons and holes in the material will be facilitated. Then, O_2 adsorption (see (3) and (4)) allows electrons' capture in material's surface generating firstly superoxide species (see (5)) and secondly the hole mobility to carry out the oxidation reaction of 2,4-D molecules by means of the generation of hydroxyl radicals (see (6) and (7)) obtaining mainly CO_2 and H_2O as degradation products. Consider

$$[Ca_{0.666}Al_{0.333}(OH)_2](A^{n-})_{x/n} \cdot mH_2O \xrightarrow{\Delta} [Ca_{24}Al_{28}O_{64}]^{4+} + 2O^{2-} \quad (2)$$

$$O_2 + 2e^- \longrightarrow 2O_2^- \quad (3)$$

$$2O_2^- + O_2 \longrightarrow 2O^- + *2O_2^- \quad (4)$$

$$[Ca_{24}Al_{28}O_{64}]^{4+} * O_2^- + H_2O \longrightarrow [Ca_{24}Al_{28}O_{64}]^{4+} + 2OH^- \quad (5)$$

$$[Ca_{24}Al_{28}O_{64}]^{4+} + 2OH^- + h\nu \longrightarrow [Ca_{24}Al_{28}O_{64}]^{4+} + 2OH^- \quad (6)$$

$$C_8H_6Cl_2O_3 + 2OH^- \longrightarrow H_2O + CO_2 \quad (7)$$

$$[Ca_{24}Al_{28}O_{64}]^{4+} + C_8H_6Cl_2O_3 \longrightarrow H_2O + CO_2 \quad (8)$$

With such materials, the photocatalytic process is conducted through photoredox reactions, so the presence of oxygen O_2^- radicals on the structure's surface generated during material's annealing will be determinant in photodegradation process since the surface oxygen radicals are the main electron acceptor species which upon contact with water will drive the formation of OH^- radicals, thus initiating the catalytic photodegradation reaction [35].

On the other side, it is been also reported that electronic deficiency generated by aluminum introduction encourages the generation of negative charges allowing water molecules' capture favoring OH^- radicals generation by photooxidation reactions [64]. Hence, after a thermal activation they are able to present photocatalytic efficiency since their negatively charged electrons reacted with dissolved oxygen to produce hydroxyl radicals which are considered as strong and nonselectively oxidizing agents of organic pollutants.

4. Conclusions

In this work, three hydrocalumite-like compounds containing nitrate and acetate anions were prepared by a sustainable method and evaluated as catalysts precursors for 2,4-dichlorophenoxyacetic acid (2,4-D) photodegradation in the presence of UV light. By the XRD and FTIR analysis the incorporation of the nitrate and acetate ions was confirmed. The XRD analysis of the calcined materials at 700°C indicated that mayenite and CaO were obtained and their relative amounts depended on the anion's nature and quantity. Although in the past these materials were not considered as

semiconductors in this work their semiconductive properties were evidenced since the best material presented a band gap value of 3.2 eV achieving a 57% degradation of 2,4-D (40 ppm) and a mineralization percentage of 60% within 150 minutes. It was demonstrated that the photocatalytic activity depended not only on the crystalline phases but also on the chemical composition and textural and optical properties. A photoredox mechanism was proposed to be responsible for initiating the photocatalytic degradation of the 2,4-D molecules together with the electronic deficiencies generated by aluminum introduction in material's structure.

Competing Interests

The authors declare that they have no competing interests.

Acknowledgments

Claudia M. Gomez thanks BUAP for the postdoctoral scholarship DSA/103.5/14/8403 granted by Programa para el Desarrollo Profesional Docente para el Tipo Superior (PRODEP). The authors also thank CUVyTT for the help given in material's analysis.

References

[1] M. Alvarez, T. López, J. A. Odriozola et al., "2,4-Dichlorophenoxyacetic acid (2,4-D) photodegradation using an M^{n+}/ZrO_2 photocatalyst: XPS, UV-vis, XRD characterization," *Applied Catalysis B: Environmental*, vol. 73, no. 1-2, pp. 34–41, 2007.

[2] Catálogo Oficial de Plaguicidas 2004 de la Comisión Intersecretarial para el Control del Proceso y Uso de Plaguicida, Fertilizantes y Sustancias Tóxicas (CICOPLAFEST), México, 2004.

[3] C. Yu, H. Wang, X. Liu et al., "Photodegradation of 2,4-D induced by NO_2^- in aqueous solutions: the role of NO_2," *Journal of Environmental Sciences*, vol. 26, no. 7, pp. 1383–1387, 2014.

[4] G. López-Granada, J. D. O. Barceinas-Sánchez, R. López, and R. Gómez, "High temperature stability of anatase in titania–alumina semiconductors with enhanced photodegradation of 2,4-dichlorophenoxyacetic acid," *Journal of Hazardous Materials*, vol. 263, no. 1, pp. 84–92, 2013.

[5] D. Fabbri, A. Crime, M. Davezza et al., "Surfactant-assisted removal of swep residues from soil and photocatalytic treatment of the washing wastes," *Applied Catalysis B: Environmental*, vol. 92, no. 3-4, pp. 318–325, 2009.

[6] A. Barrera, F. Tzompantzi, V. Lara, and R. Gómez, "Photodegradation of 2,4-D over PdO/Al_2O_3-Nd_2O_3 photocatalysts prepared by the sol-gel method," *Journal of Photochemistry and Photobiology A: Chemistry*, vol. 227, no. 1, pp. 45–50, 2012.

[7] G. Jácome-Acatitla, F. Tzompantzi, R. López-González, C. García-Mendoza, J. M. Alvaro, and R. Gómez, "Photodegradation of sodium naproxen and oxytetracycline hydrochloride in aqueous medium using as photocatalysts Mg-Al calcined hydrotalcites," *Journal of Photochemistry and Photobiology A: Chemistry*, vol. 277, pp. 82–89, 2014.

[8] K. Dutta, S. Das, and A. Pramanik, "Concomitant synthesis of highly crystalline Zn–Al layered double hydroxide and ZnO: phase interconversion and enhanced photocatalytic activity," *Journal of Colloid and Interface Science*, vol. 366, no. 1, pp. 28–36, 2012.

[9] K. M. Parida and L. Mohapatra, "Carbonate intercalated Zn/Fe layered double hydroxide: a novel photocatalyst for the enhanced photo degradation of azo dyes," *Chemical Engineering Journal*, vol. 179, pp. 131–139, 2012.

[10] Z. Bouberka, K. A. Benabbou, A. Khenifi, and U. Maschke, "Degradation by irradiation of an Acid Orange 7 on colloidal TiO_2/(LDHs)," *Journal of Photochemistry and Photobiology A: Chemistry*, vol. 275, pp. 21–29, 2014.

[11] X. Liu, X. Zhao, Y. Zhu, and F. Zhang, "Experimental and theoretical investigation into the elimination of organic pollutants from solution by layered double hydroxides," *Applied Catalysis B: Environmental*, vol. 140-141, pp. 241–248, 2013.

[12] L. Tian, Y. Zhao, S. He, M. Wei, and X. Duan, "Immobilized Cu–Cr layered double hydroxide films with visible-light responsive photocatalysis for organic pollutants," *Chemical Engineering Journal*, vol. 184, pp. 261–267, 2012.

[13] G. Mendoza-Damián, F. Tzompantzi, A. Mantilla, A. Barrera, and L. Lartundo-Rojas, "Photocatalytic degradation of 2,4-dichlorophenol with MgAlTi mixed oxides catalysts obtained from layered double hydroxides," *Journal of Hazardous Materials*, vol. 263, pp. 67–72, 2013.

[14] A. Mantilla, F. Tzompantzi, J. L. Fernández, J. A. I. Díaz Góngora, G. Mendoza, and R. Gómez, "Photodegradation of 2,4-dichlorophenoxyacetic acid using ZnAlFe layered double hydroxides as photocatalysts," *Catalysis Today*, vol. 148, no. 1-2, pp. 119–123, 2009.

[15] F. Tzompantzi, G. Mendoza-Damián, J. L. Rico, and A. Mantilla, "Enhanced photoactivity for the phenol mineralization on ZnAlLa mixed oxides prepared from calcined LDHs," *Catalysis Today*, vol. 220–222, pp. 56–60, 2014.

[16] J. S. Valente, F. Tzompantzi, J. Prince, J. G. H. Cortez, and R. Gomez, "Adsorption and photocatalytic degradation of phenol and 2,4 dichlorophenoxiacetic acid by Mg–Zn–Al layered double hydroxides," *Applied Catalysis B: Environmental*, vol. 90, no. 3-4, pp. 330–338, 2009.

[17] R. K. Sahu, B. S. Mohanta, and N. N. Das, "Synthesis, characterization and photocatalytic activity of mixed oxides derived from ZnAlTi ternary layered double hydroxides," *Journal of Physics and Chemistry of Solids*, vol. 74, no. 9, pp. 1263–1270, 2013.

[18] L. Huang, S. Chu, J. Wang et al., "Novel visible light driven Mg-Zn-In ternary layered materials for photocatalytic degradation of methylene blue," *Catalysis Today*, vol. 212, pp. 81–88, 2013.

[19] M. J. Campos-Molina, J. Santamaría-Gonźalez, J. Mérida-Robles et al., "Base catalysts derived from hydrocalumite for the transesterification of sunflower oil," *Energy & Fuels*, vol. 24, no. 2, pp. 979–984, 2010.

[20] M. Sánchez-Cantú, L. M. Pérez-Díaz, N. Tepale-Ochoa et al., "Green synthesis of hydrocalumite-type compounds and their evaluation in the transesterification of castor bean oil and methanol," *Fuel*, vol. 110, pp. 23–31, 2013.

[21] I. Cota, E. Ramírez, F. Medina, J. E. Sueiras, G. Layrac, and D. Tichit, "New synthesis route of hydrocalumite-type materials and their application as basic catalysts for aldol condensation," *Applied Clay Science*, vol. 50, no. 4, pp. 498–502, 2010.

[22] Y. Kuwahara and H. Yamashita, "A new catalytic opportunity for waste materials: application of waste slag based catalyst in CO_2 fixation reaction," *Journal of CO2 Utilization*, vol. 1, pp. 50–59, 2013.

[23] E. López-Salinas, M. E. L. Serrano, M. A. C. Jácome, and I. S. Secora, "Characterization of synthetic hydrocalumite-type

$[Ca_2Al(OH)_6]NO_3 \cdot mH_2O$: effect of the calcination temperature," *Journal of Porous Materials*, vol. 2, no. 4, pp. 291–297, 1996.

[24] M. A. Aramendía, V. Borau, C. Jiménez, J. M. Marinas, J. R. Ruiz, and F. J. Urbano, "Activity of basic catalysts in the Meerwein-Ponndorf-Verley reaction of benzaldehyde with ethanol," *Journal of Colloid and Interface Science*, vol. 238, no. 2, pp. 385–389, 2001.

[25] M. François, G. Renaudin, and O. Evrard, "A cementitious compound with composition $3CaO.Al_2O_3$-$CaCO_3$.$11H_2O$," *Acta Crystallographica Section C: Crystal Structure Communications*, vol. 54, no. 9, pp. 1214–1217, 1998.

[26] P. Zhang, G. Qian, Z. P. Xu et al., "Effective adsorption of sodium dodecylsulfate (SDS) by hydrocalumite (CaAl-LDH-Cl) induced by self-dissolution and re-precipitation mechanism," *Journal of Colloid and Interface Science*, vol. 367, no. 1, pp. 264–271, 2012.

[27] Y. Li, J. Wang, Z. Li et al., "Ultrasound assisted synthesis of Ca-Al hydrotalcite for U (VI) and Cr (VI) adsorption," *Chemical Engineering Journal*, vol. 218, pp. 295–302, 2013.

[28] E. Pérez-Barrado, M. C. Pujol, M. Aguiló et al., "Fast aging treatment for the synthesis of hydrocalumites using microwaves," *Applied Clay Science*, vol. 80-81, pp. 313–319, 2013.

[29] M. Mora, M. I. López, C. Jiménez-Sanchidrián, and J. R. Ruiz, "Ca/Al mixed oxides as catalysts for the meerwein-ponndorf-verley reaction," *Catalysis Letters*, vol. 136, no. 3-4, pp. 192–198, 2010.

[30] S. Xu, Z. Chen, B. Zhang, J. Yu, F. Zhang, and D. G. Evans, "Facile preparation of pure CaAl-layered double hydroxides and their application as a hardening accelerator in concrete," *Chemical Engineering Journal*, vol. 155, no. 3, pp. 881–885, 2009.

[31] S. Xu, B. Zhang, Z. Chen, J. Yu, D. G. Evans, and F. Zhang, "A general and scalable formulation of pure CaAl-layered double hydroxide via an organic/water solution route," *Industrial and Engineering Chemistry Research*, vol. 50, no. 11, pp. 6567–6572, 2011.

[32] L. Vieille, I. Rousselot, F. Leroux, J.-P. Besse, and C. Taviot-Guého, "Hydrocalumite and its polymer derivatives. 1. Reversible thermal behavior of friedel's salt: a direct observation by means of high-temperature in situ powder X-ray diffraction," *Chemistry of Materials*, vol. 15, no. 23, pp. 4361–4368, 2003.

[33] J. S. Valente, M. S. Cantu, and F. Figueras, "A simple environmentally friendly method to prepare versatile hydrotalcite-like compounds," *Chemistry of Materials*, vol. 20, no. 4, pp. 1230–1232, 2008.

[34] J. S. Valente, M. Sánchez-Cantú, E. Lima, and F. Figueras, "Method for large-scale production of multimetallic layered double hydroxides: formation mechanism discernment," *Chemistry of Materials*, vol. 21, no. 24, pp. 5809–5818, 2009.

[35] S. Matsuishi, Y. Toda, M. Miyakawa et al., "High-density electron anions in a nanoporous single crystal: $[Ca_{24}Al_{28}O_{64}]^{4+}(4e^-)$," *Science*, vol. 301, no. 5633, pp. 626–629, 2003.

[36] J. L. Dye, "Electrons as anions," *Science*, vol. 301, no. 5633, pp. 607–608, 2003.

[37] L. Palacios, Á. G. De La Torre, S. Bruque et al., "Crystal structures and in-situ formation study of mayenite electrides," *Inorganic Chemistry*, vol. 46, no. 10, pp. 4167–4176, 2007.

[38] D. Cruz, H. Pfeiffer, and S. Bulbulian, "Synthesis of Li_2MO_3 (M = Ti or Zr) by the combustion method," *Solid State Sciences*, vol. 8, no. 5, pp. 470–475, 2006.

[39] U. Zavyalova, B. Nigrovski, K. Pollok et al., "Gel-combustion synthesis of nanocrystalline spinel catalysts for VOCs elimination," *Applied Catalysis B: Environmental*, vol. 83, no. 3-4, pp. 221–228, 2008.

[40] J. Jimenez-Becerril, P. Bosch, and S. Bulbulian, "Synthesis and characterization of γ-$LiAlO_2$," *Journal of Nuclear Materials*, vol. 185, no. 3, pp. 304–307, 1991.

[41] V. Prevot, V. Briois, J. Cellier, C. Forano, and F. Leroux, "An in-situ investigation of LDH-acetate prepared in polyol, under moderate thermal treatment," *Journal of Physics and Chemistry of Solids*, vol. 69, no. 5-6, pp. 1091–1094, 2008.

[42] G. V. Manohara, P. Vishnu Kamath, and W. Milius, "Reversible hydration and aqueous exfoliation of the acetate-intercalated layered double hydroxide of Ni and Al: observation of an ordered interstratified phase," *Journal of Solid State Chemistry*, vol. 196, pp. 356–361, 2012.

[43] A. V. Radha, P. V. Kamath, and C. Shivakumara, "Mechanism of the anion exchange reactions of the layered double hydroxides (LDHs) of Ca and Mg with Al," *Solid State Sciences*, vol. 7, no. 10, pp. 1180–1187, 2005.

[44] L. Vieille, E. M. Moujahid, C. Taviot-Guého, J. Cellier, J.-P. Besse, and F. Leroux, "In situ polymerization of interleaved monomers: a comparative study between hydrotalcite and hydrocalumite host structures," *Journal of Physics and Chemistry of Solids*, vol. 65, no. 2-3, pp. 385–393, 2004.

[45] M. C. Gastuche, G. Brown, and M. M. Mortland, "Mixed magnesium-aluminium hydroxides I. Preparation and characterization of compounds formed in dialysed systems," *Clay Minerals*, vol. 7, no. 2, pp. 177–192, 1967.

[46] M. Sánchez-Cantú, S. Camargo-Martínez, L. M. Pérez-Díaz, M. E. Hernández-Torres, E. Rubio-Rosas, and J. S. Valente, "Innovative method for hydrocalumite-like compounds' preparation and their evaluation in the transesterification reaction," *Applied Clay Science*, vol. 114, pp. 509–516, 2015.

[47] P. Zhang, G. Qian, H. Cheng, J. Yang, H. Shi, and R. L. Frost, "Near-infrared and mid-infrared investigations of Na-dodecylbenzenesulfate intercalated into hydrocalumite chloride (CaAl-LDH-Cl)," *Spectrochimica Acta Part A: Molecular and Biomolecular Spectroscopy*, vol. 79, no. 3, pp. 548–553, 2011.

[48] Y. Yang, X. Zhao, Y. Zhu, and F. Zhang, "Transformation mechanism of magnesium and aluminum precursor solution into crystallites of layered double hydroxide," *Chemistry of Materials*, vol. 24, no. 1, pp. 81–87, 2012.

[49] Y. Kuwahara, K. Tsuji, T. Ohmichi, T. Kamegawa, K. Mori, and H. Yamashita, "Transesterifications using a hydrocalumite synthesized from waste slag: an economical and ecological route for biofuel production," *Catalysis Science and Technology*, vol. 2, no. 9, pp. 1842–1851, 2012.

[50] M. J. Hernandez-Moreno, M. A. Ulibarri, J. L. Rendon, and C. J. Serna, "IR characteristics of hydrotalcite-like compounds," *Physics and Chemistry of Minerals*, vol. 12, no. 1, pp. 34–38, 1985.

[51] P. Zhang, G. Qian, H. Shi, X. Ruan, J. Yang, and R. L. Frost, "Corrigendum to 'Mechanism of interaction of hydrocalumites (Ca/Al-LDH) with methyl orange and acidic scarlet GR' [JCIS 365 (2012) 110-116]," *Journal of Colloid and Interface Science*, vol. 367, no. 1, p. 540, 2012.

[52] Z. P. Xu and P. S. Braterman, "Synthesis, structure and morphology of organic layered double hydroxide (LDH) hybrids: comparison between aliphatic anions and their oxygenated analogs," *Applied Clay Science*, vol. 48, no. 1-2, pp. 235–242, 2010.

[53] S. K. Yun and T. J. Pinnavaia, "Water content and particle texture of synthetic hydrotalcite-like layered double hydroxides," *Chemistry of Materials*, vol. 7, no. 2, pp. 348–354, 1995.

[54] G. Renaudin, J.-P. Rapin, B. Humbert, and M. François, "Thermal behaviour of the nitrated AFm phase $Ca_4Al_2(OH)_{12}(NO_3)_2 \cdot 4H_2O$ and structure determination of the intermediate hydrate $Ca_4Al_2(OH)_{12}(NO_3)_2 \cdot 2H_2O$," *Cement and Concrete Research*, vol. 30, no. 2, pp. 307–314, 2000.

[55] E. Kandare and J. M. Hossenlopp, "Thermal degradation of acetate-intercalated hydroxy double and layered hydroxy salts," *Inorganic Chemistry*, vol. 45, no. 9, pp. 3766–3773, 2006.

[56] M. Sánchez-Cantú, L. M. Pérez-Díaz, R. Rosales et al., "Commercial hydrated lime as a cost-effective solid base for the transesterification of wasted soybean oil with methanol for biodiesel production," *Energy and Fuels*, vol. 25, no. 7, pp. 3275–3282, 2011.

[57] C. R. Milne, G. D. Silcox, D. W. Pershing, and D. A. Kirchgessner, "Calcination and sintering models for application to high-temperature, short-time sulfation of calcium-based sorbents," *Industrial and Engineering Chemistry Research*, vol. 29, no. 2, pp. 139–149, 1990.

[58] C. Li, D. Hirabayashi, and K. Suzuki, "Synthesis of higher surface area mayenite by hydrothermal method," *Materials Research Bulletin*, vol. 46, no. 8, pp. 1307–1310, 2011.

[59] F. Rouquerol, J. Rouquerol, and K. Sing, *Adsorption by Powders and Porous Solids—Principles, Methodology and Applications*, Academic Press, San Diego, Calif, USA, 1999.

[60] S. Sankaranarayanan, C. A. Antonyraj, and S. Kannan, "Transesterification of edible, non-edible and used cooking oils for biodiesel production using calcined layered double hydroxides as reusable base catalysts," *Bioresource Technology*, vol. 109, pp. 57–62, 2012.

[61] B. Pourabbas and B. Jamshidi, "Preparation of MoS_2 nanoparticles by a modified hydrothermal method and the photocatalytic activity of MoS_2/TiO_2 hybrids in photo-oxidation of phenol," *Chemical Engineering Journal*, vol. 138, no. 1–3, pp. 55–62, 2008.

[62] N. Morales-Flores, U. Pal, and E. Sánchez-Mora, "Photocatalytic behavior of ZnO and Pt-incorporated ZnO nanoparticles in phenol degradation," *Applied Catalysis A: General*, vol. 394, no. 1-2, pp. 269–275, 2011.

[63] J. Prince, F. Tzompantzi, G. Mendoza-Damián, F. Hernández-Beltrán, and J. S. Valente, "Photocatalytic degradation of phenol by semiconducting mixed oxides derived from Zn(Ga)Al layered double hydroxides," *Applied Catalysis B: Environmental*, vol. 163, pp. 352–360, 2015.

[64] K. R. Nemade and S. A. Waghuley, "Low temperature synthesis of semiconducting α-Al_2O_3 quantum dots," *Ceramics International*, vol. 40, no. 4, pp. 6109–6113, 2014.